J. Membrane Biol. 191, 179–192 (2003)
DOI: 10.1007/s00232-002-1054-0

The Journal of
Membrane
Biology

Ca^{2+} Dynamics during Membrane Excitation of Green Alga *Chara*: Model Simulations and Experimental Data

M. Wacke, G. Thiel, M.-T. Hütt
Institute for Botany, Plant Biophysics, Darmstadt University of Technology, Schnittspahnstr. 3, D-64287, Darmstadt, Germany

Received: 8 July 2002/Revised: 21 October 2002

Abstract. Kinetic investigations of stimulus response coupling in the green alga *Chara* have revealed that an intermediate second messenger is formed in the process of membrane excitation. This second messenger links electrical stimulation to the mobilization of Ca^{2+} from internal stores. In the present work, the experimentally based kinetic model, which describes the stimulus-dependent production of the second messenger and Ca^{2+} mobilization, is combined with a model for inositol 1,4,5-trisphosphate (IP_3)-and Ca^{2+}-sensitive gating of a Ca^{2+}-release channel in endomembranes of animal cells. The combination of models allows a good simulation of experimental data, including the all-or-none-type dependence of the Ca^{2+} response on stimulus duration and complex phase locking phenomena for the dependence of the Ca^{2+} response on stimulation frequency. The model offers a molecular explanation for the refractory phenomenon in *Chara*, assigning it to the life time of an inactive state of the Ca^{2+}-release channel. The model furthermore explains the steep dependence of excitation on strength/duration of electrical stimulation as a consequence of an interplay of the dynamical variables in the model.

Key words: Calcium mobilization — *Chara* action potential — Inostitol-1,4,5,-trisphosphate (IP_3) metabolism — Refraction period — Model simulation

Introduction

The membrane of the giant alga *Chara* is electrically excitable. Central to this electrical excitation is that depolarizing electrical stimuli evoke a transient elevation in the concentration of free Ca^{2+} in the cytoplasm ($[Ca^{2+}]_{cyt}$). This in turn leads to an activation of Ca^{2+}-sensitive Cl^- channels and hence initiates membrane depolarization (for review, *see* Tazawa, Shimmen & Mimura, 1987; Thiel, Homann & Plieth, 1997).

Recently, details of the stimulus response coupling were uncovered by the analysis of the relation between the electrical stimulation and the Ca^{2+} response. Monitoring cytoplasmic Ca^{2+} in response to graded electrical stimulations showed a sharp threshold for the Ca^{2+} response with respect to the strength/duration of electrical stimulation (Wacke & Thiel 2001). While small pulses failed to evoke any perceivable change in $[Ca^{2+}]_{cyt}$, the entire Ca^{2+} response was stimulated after passing a narrow threshold. Further details on the link between the electrical stimulation and $[Ca^{2+}]_{cyt}$ were derived from experiments in which the Ca^{2+} response was evoked by trains of subthreshold pulses (Wacke & Thiel 2001). These experiments showed an additive effect of individual stimulation pulses with the consequence that small, otherwise ineffective pulses were able to evoke — when applied in an appropriate regime — the entire Ca^{2+} response on the last pulse. These findings suggested the involvement of a long-lived signaling molecule, which is produced in a voltage-dependent manner and is able to mobilize Ca^{2+} internal stores. This interpretation is in good agreement with other experiments, which had already suggested from independent approaches that electrical excitation in *Chara* is due to a mobilization of Ca^{2+} from internal stores (Plieth et al., 1998, Thiel & Dityatev, 1998), and may be mediated by the second messenger inositol 1,4,5-trisphosphate (IP_3) (Thiel, MacRobbie & Henke, 1990; Biskup, Gradmann & Thiel, 1999; Wacke & Thiel, 2001).

All experimental observations in the context of Ca^{2+} responses to graded electrical stimuli could be successfully simulated by a model based on the

Correspondence to: G. Thiel; email: thiel@bio.tu-darmstadt.de

Abbreviations: action potential, AP; inositol-1,4,5,-trisphosphate, IP_3; phosphatidyl inositol(4,5) bisphosphate, PIP_2.

voltage-dependent production of a second messenger (Wacke & Thiel 2001). According to this model, Ca^{2+} is liberated from internal stores in an all-or-none manner once a critical concentration (threshold) of the second messenger is exceeded in the cytoplasm. In the case of a subthreshold pulse, the concentration of this molecule remains under the critical threshold for Ca^{2+} mobilization. Messenger molecules newly formed in a second stimulation are added to the remains from the first stimulation and in this way, two sub-threshold pulses can act in an additive manner to elevate the signaling molecule above a critical value and stimulate Ca^{2+} release from internal stores.

While this model provides a good quantitative description for the dependence of Ca^{2+} mobilization on the voltage-sensitive production of a second messenger, it neither explains the nature of the threshold nor does it account for phenomena such as refractory behavior (Beilby & Coster, 1979) and temporal patterns of excitation.

In the present work, we present a combination of our previous model and an established model on the concerted action of IP_3 and Ca^{2+} for the liberation of Ca^{2+} from internal stores in animal cell (Tang, Stephenson & Othmer, 1996; Othmer, 1997). Numerical simulations with the combined model now reveal that the experimentally detected threshold results from the interplay between the dynamical variables and is an intrinsic threshold in the model. Furthermore, the model simulations were also used as guidelines for further experiments on periodic electrical stimulation of *Chara*. We found in model simulations as well as experimentally that the amount of Ca^{2+} that is liberated in a stimulation, decreases and the frequency with which the cell responds to stimulations vanishes with increasing frequency of stimulation. This provides essentially a molecular understanding for the phenomenon of refraction periods in membrane excitation of *Chara*.

Materials and Methods

Cell materials and experimental procedures were the same as those reported in Wacke &Thiel (2001).

The Model

As a starting point we use a mathematical model of Ca^{2+} dynamics developed by Othmer (1997). There, the main aim was to understand, how IP_3 influences Ca^{2+} dynamics in endothelial cells. Based upon previous work (Wacke & Thiel, 2001), we could formulate an addition to this model, leading to a different biological focus. The additional differential equation, which inserts IP_3 as a dynamical variable rather than as an external parameter, now allows us to study the mathematical model of Ca^{2+} dynamics as a function of external voltage stimuli. This shift in biological focus has two important effects. First, it enables us to directly compare our experimental findings on *Chara* with the model simulations. Second, the new model displays a much richer repertoire of dynamics under periodic stimulation, including chaotic amplitude modulations. While we will discuss the first point in detail, we will only hint at the second point and leave a detailed stability analysis and a comparison of the two models with methods from nonlinear dynamics for future work.

Othmer (1997) described the relation between the cytoplasmic concentration of IP_3 and the $[Ca^{2+}]_{cyt}$ by using a four-state model for an IP_3-sensitive Ca^{2+} channel in the membrane of the endoplasmic reticulum. This channel is the assumed pathway for ligand-activated release of Ca^{2+} from cytoplasmic stores. The four states of the receptor are unbound (R), bound to IP_3 molecule (RI), bound to the IP_3 molecule and a first, activating Ca^{2+} ion (RIC_+) and finally a state where the receptor is bound additionally to a second, deactivating Ca^{2+} ion (RIC_+C_-). The channel is only conductive when the receptor is in the RIC_+ state. The binding order of the ions and molecules to the receptor is not free. For simplicity of notation we replace $[Ca^{2+}]_{cyt}$ by C and $[IP_3]_{cyt}$ by I in the following reaction scheme and equations.

In terms of concentrations, the state transition scheme is that given by

$$\begin{aligned} R + I &\underset{k_{-1}}{\overset{k_1}{\rightleftarrows}} RI \\ RI + C &\underset{k_{-2}}{\overset{k_2}{\rightleftarrows}} RIC \\ RIC_+ + C &\underset{k_{-3}}{\overset{k_3}{\rightleftarrows}} RC_+IC_- \end{aligned} \tag{1}$$

in which the k_i, ($i = \pm1, \pm2, \pm3$) are the rate constants of the state transitions.

The transport of Ca^{2+} from the cytoplasm back into the sacroplasmic reticulum, forced by an endogeneous Ca^{2+} pump, which can be described by a Hill function:

$$\bar{g}(C) = \frac{\bar{p}_1 C^4}{C^4 + \bar{p}_2^4} \tag{2}$$

In this equation $g(C)$ is the Ca^{2+} conductance, $\bar{p}_1$ and $\bar{p}_2$ are the Hill coefficients. For details, *see* Othmer (1997).

Let x_i ($i = 2,...,5$) denote the fractions in states R, RI, RIC_+, RIC_+C_-, respectively. We then define $x_1 = C/C_0$ with the volume average calcium concentration C_0. Othmer (1997) defined

$$C_0 = \frac{C + v_r C_s}{(1 + v_r)} \tag{3}$$

in which C_s is the calcium concentration in the store and v_r the ratio of the ER volume to the volume of the cytoplasm. Defining $\lambda...1 + v_r$, $\bar{k}_2 = \bar{k}_2 \bar{C}_0$, $k_3 = k_3 C_0$, $p_1 = \bar{p}_1/C_0$ and $p_2 = \bar{p}_2/C_0$, Othmer's model (Othmer, 1997) is given by the five coupled nonlinear differential equations:

$$\begin{aligned} \frac{dx_1}{dt} &= \lambda(\gamma_0 + \gamma_1 x_4)(1 - x_1) - \frac{p_1 {x_1}^4}{p_2^4 + x_1^4}, \\ \frac{dx_2}{dt} &= -k_1 I x_2 + k_{-1} x_3, \\ \frac{dx_3}{dt} &= -(k_{-1} + k_2 x_1) x_3 + k_1 I x_2 + k_{-2} x_4, \\ \frac{dx_4}{dt} &= k_2 x_1 x_3 + k_{-3} x_5 - (k_{-2} + k_3 x_1) x_4, \\ \frac{dx_5}{dt} &= k_3 x_1 x_4 - k_{-3} x_5. \end{aligned} \tag{4}$$

γ_0 is the basal permeability of the Ca^{2+} store membrane in the absence of IP_3 and γ_1, the density of IP_3-sensitive channels, both per unit volume of the Ca^{2+} stores.

In this scaling, all x_i range between 0 and 1. Eq. 4 fulfills a conservation condition $\sum_{k=2}^{5} X_k = 1$, which expresses the fact that each receptor has to be in one of the four states.

While Othmer (1997) used the IP_3 concentration as a parameter, we treated IP_3 as a dynamical variable. In Wacke and Thiel (2001) we presented two coupled linear differential equations to describe a voltage-dependent IP_3 production:

$$\frac{f[Q_1]_t}{ft} = k_{Q1}([Q_1]_0 - [Q_1]_t) - k_{Q2}[Q_1]_t \quad (5)$$

$$\frac{f[Q_2]_t}{ft} = k_{Q2}([Q_1]_t - k_{Q3}[Q_2]_t. \quad (6)$$

Here we identify Q_2 with IP_3 and consequently Q_1 with phosphatidylinositol, 4,5-bisphosphate (PIP_2), which is the known predecessor of IP_3. Furthermore, for simplification we assume in the present case PIP_2 as constant, so we can eliminate Eq. 5 from our system. This assumption is justified by the experimental observation that short stimulation pulses can only deplete the PIP_2 pool when multiple pulses are applied with high (≥1 Hz) frequency (Wacke & Thiel 2001). In all experiments presented here, the pulses were applied at much lower frequencies. Nevertheless, it should be kept in mind that for the simulation of all phenomena related to electrical stimulation with one model, it is necessary to use Q_1 as variable and keep Eq. 5 in the system (*see* Wacke & Thiel, 2001).

Previously we defined

$$k_{Q2} = \frac{c_2(i - i_0)}{q}$$

for $i - i_0 > 0$ and $k_{Q_2} = 0$ for $i \le i_0$, (Wacke & Thiel 2001). In this equation, i is the current of the pulse, i_0 is the experimental fixed minimum current that an infinite pulse must have to evoke any effect on the cytoplasmic IP_3, q is the minimum charge to be transported for effective excitation of the cell, and c_2, a dimensionless fitting parameter. Here we define $k_4 = \frac{c_2[Q_1]}{q}$ with the dimension $Mol \cdot C^{-1}$. k_4 is then a measure for the current-dependent production of IP_3, and with

$$f(i) = \begin{cases} \left(1 - \frac{i_0}{i}\right) & \text{if } \frac{i}{i_0} > 1, \\ 0 & \text{else} \end{cases} \quad (7)$$

and $k_{Q_3} = k_{-4}$ we can write Eq. 6 as

$$\frac{dI}{dt} = k_4 f(i) i - k_{-4} I. \quad (8)$$

This additional equation, which describes IP_3 production and depletion, has been added to the model from Othmer (1997). $[IP_3]_{cyt}$ is no longer the input signal or the output signal. Instead, the input signal is, like in the real experiments, the external current protocol and the output signal is $[Ca^{2+}]_{cyt}$.

For numerical integration of the six differential equations we used a 6th order Runge-Kutta algorithm, as described in Press et al. (1988).

Determination of the Parameters

Because we wanted to preserve the dynamics of the previous model, we took all parameter values in Eq. 4 from Othmer (1997) except the value of k_{-3}. For the discussion of the chosen values of k_{-3}, *see* Results and Discussion. The size of k_{-4} was determined by Wacke and Thiel (2001), as well as the value of i_0. Finally, we used k_4 to fit our model to the threshold for evoking a transient rise of Ca^{2+} we had found in previous experiments (Wacke & Thiel 2001). All values are listed in Table 1.

Table 1. Model parameters used for numerical integration of Eqs. 4 and 8.

Parameter	Value	Parameter	Value
v_r	0.185	k_1	12.0 (μM sec)$^{-1}$
γ_0	0.1 sec^{-1}	k_2	15.0 (μM sec)$^{-1}$
γ_1	20.5 sec^{-1}	k_3	1.8 (μM sec)$^{-1}$
p_1	8.5 μM sec^{-1}	k_4	21.5 MC^{-1}
p_2	0.065 μM	k_{-1}	8.0 sec^{-1}
C_0	1.56 μM	k_{-2}	1.65 sec^{-1}
i_0	2.5 μA	k_{-3}	0.04...0.086 sec^{-1}
		k_{-4}	0.2 sec^{-1}

Results and Discussion

The Model Implies a Threshold for the IP_3 Concentration

Figure 1 shows six simulated Ca^{2+} responses, which were evoked by pulses with different length but identical strength. Before onset of each pulse, the system was allowed to equilibrate for 90 seconds. Pulses shorter than about 48 msec have no or little effect on $[Ca^{2+}]_{cyt}$. Pulses with a longer duration result in Ca^{2+} responses with a much larger amplitude. Over a very narrow window of pulse duration (48–50 msec) only small increases in pulse duration result in drastic increases in the Ca^{2+}-response amplitude, which saturates at pulse durations of longer than about 50 msec

The simulation illustrates that in our model, the pulse duration also affects the kinetics of the Ca^{2+} response. With increasing pulse duration, the $[Ca^{2+}]_{cyt}$ peak shifted towards the onset of the stimulation pulse and the rise in $[Ca^{2+}]_{cyt}$ is accelerated.

Figure 2 shows the corresponding Ca^{2+} responses when the pulse duration is kept constant but the pulse strength is varied. In essence, the result is very similar to that presented in Fig. 1 in the sense that the ΔCa^{2+} response reveals a critical window of pulse strengths, in which small changes in pulse duration result in a large effect on the Ca^{2+} response amplitude.

Figure 3*A* summarizes this result. There, the difference $[\Delta Ca^{2+}]_{cyt}$ between the equilibrium $[Ca^{2+}]_{cyt}$ and the maximal $[Ca^{2+}]_{cyt}$ is plotted versus the pulse strength. By equilibrium $[Ca^{2+}]$ we understand the Ca^{2+} concentration approached a long time (=90 sec) after the pulse. The curve is a linear interpolation from 37 simulations such as those shown in Fig. 2.

The plot illustrates that in order to evoke a significant Ca^{2+} response, current pulses clearly have to

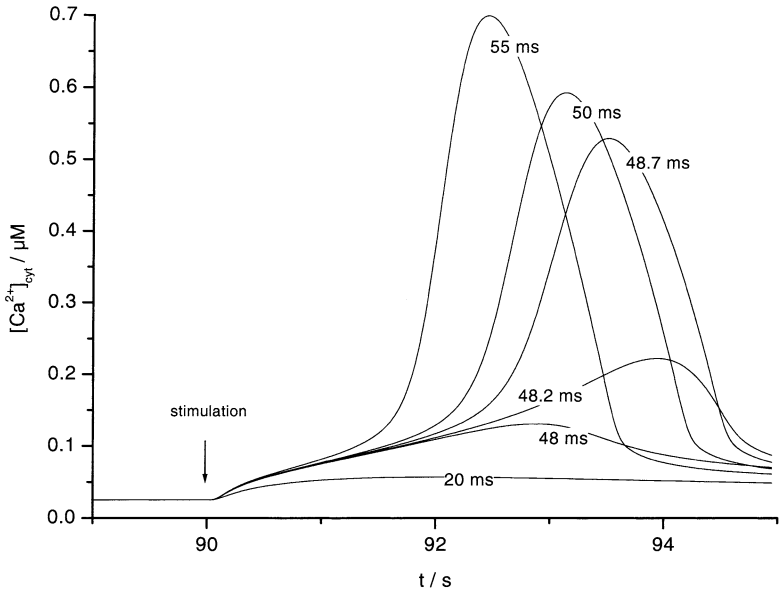

Fig. 1. Effect of pulse duration on the simulated Ca^{2+} response. Six simulated Ca^{2+} transients evoked by pulses with constant strength (5 µA) and variable durations (indicated on trajectories). All pulses were started after 90 seconds, during which time the system equilibrated. The value of k_{-3} was 0.086 sec^{-1}. For values of the remaining parameters, *see* Table 1.

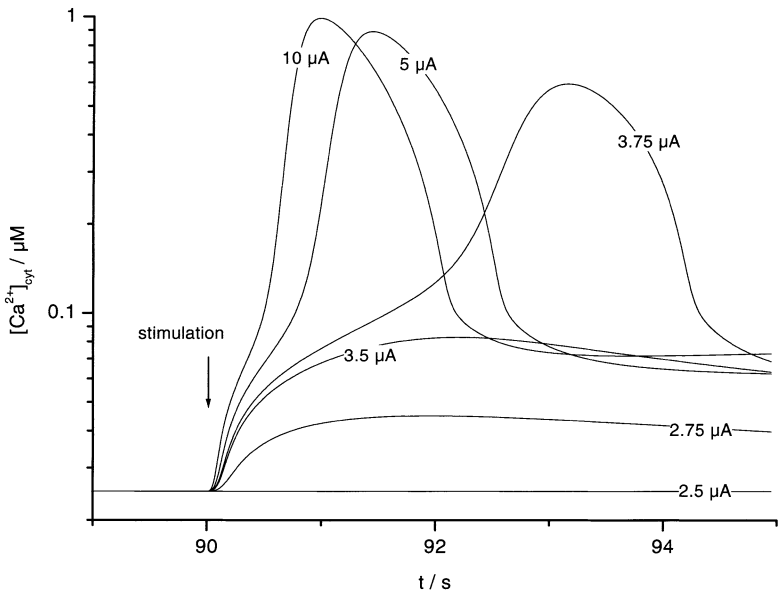

Fig. 2. Effect of pulse strength on simulated $[Ca^{2+}]_{cyt}$ transients. Six simulated Ca^{2+} transients evoked by pulses with constant duration (100 msec) and variable strength (indicated on trajectories). All pulses were started after 90 seconds, during which time the system equilibrated. The value of k_{-3} was 0.086 sec^{-1}. For values of the remaining parameters, *see* Table 1.

be stronger than $i_0 = 2.5$ µA. This first threshold is seen as a first deviation from zero of the Ca^{2+} curve and is already implied by Eq. 7. However, the system displays a second threshold i_0^* (3.7 µA, Fig. 3*A*, at the position of the steep increase in $[Ca^{2+}]_{cyt}$), which cannot immediately be predicted from the differential equations themselves. Indeed, this second threshold is the result of the interplay of several dynamical components of the system, as discussed below. The model evidently implies a quasi all-or-none mechanism for electrical stimulation of $[Ca^{2+}]_{cyt}$ elevation.

In Figure 3*B*, the model simulations are compared with experimental data. For comparison, the simulated and measured data were normalized as described in the figure legend. The plot illustrates that the all-or-none Ca^{2+} response predicted by the model (Fig. 3*A*) is in agreement with the experimental results from Wacke & Thiel (2001).

Figure 4*A* illustrates the fact, that the threshold, which is generated by Eqs. 4 and 8, is a threshold in $[IP_3]$. From 37 simulations such as in Fig. 2, the difference between the equilibrium $[Ca^{2+}]_{cyt}$ and the maximal $[Ca^{2+}]_{cyt}$ is plotted versus the simulated maximum of $[IP_3]$.

The relation between $[IP_3]$ and the Ca^{2+}-response amplitude shows a similar sigmoidal behavior. This is due to the linear nature of Eq. 8, which connects the IP_3 production to the current amplitude of the stimulation pulse. It, however, demonstrates that our model goes beyond the one discussed in Wacke and

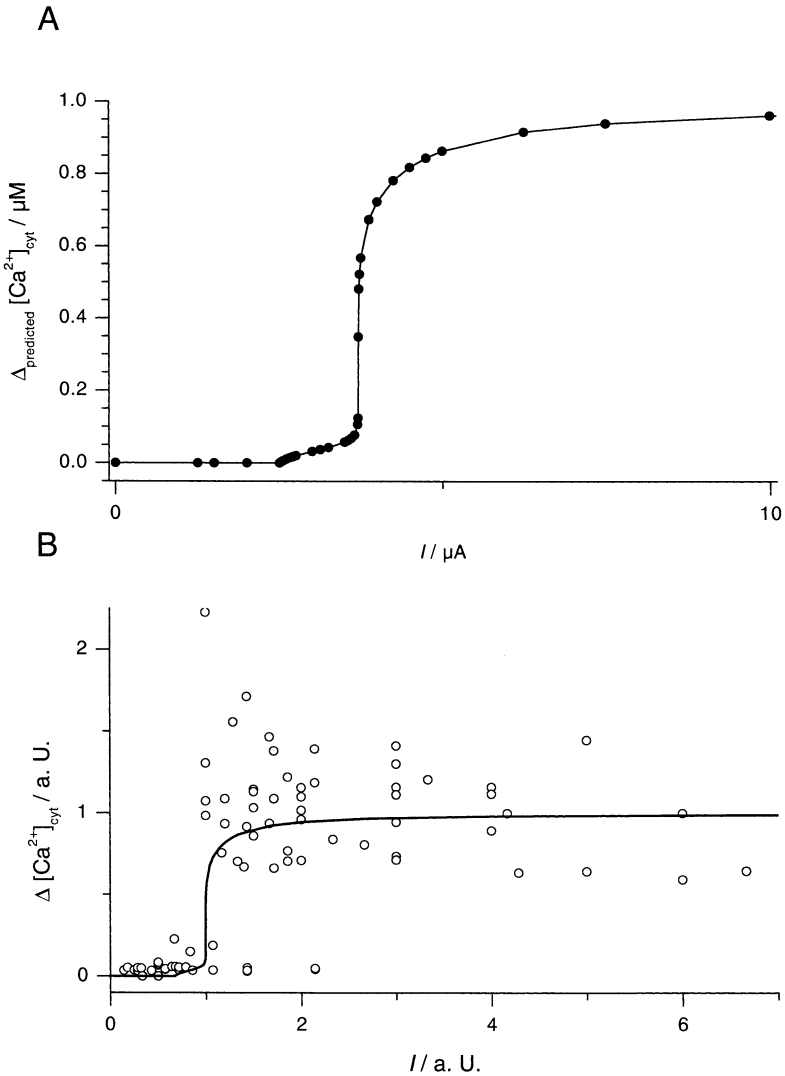

Fig. 3. The experimentally measured all-or-none behavior for stimulus-induced Ca^{2+} responses is reproduced by the model. (*A*) From 31 simulations such as in Fig. 2 with pulse strength between 0 and 25 µA, the maximal $[Ca^{2+}]_{cyt}$ response was obtained. The smooth curve obtained by linear interpolation between calculated points. (*B*) Comparison of simulated (line) and experimentally measured $[Ca^{2+}]_{cyt}$ responses (empty symbols) in response to stimuli with different strength. For comparison the experimental and simulated data were normalized. In the case of the experimental data, the smallest pulse that evoked a Ca^{2+} response in 3 cells investigated was taken as unity for the pulse strength. The mean maximal Ca^{2+} response was taken as unity for the response amplitude. From simulations of Ca^{2+} responses, a maximal response amplitude of 1.02 µM Ca^{2+} was estimated for pulses with infinite strength. This value was defined as unity. The pulse strength obtained in simulations such as in Fig. 2 as half asymptote value was set as the pulse strength unity.

Thiel (2001). There, such a threshold was one of the main assumptions. In this way, the model described here now gives a detailed account of how this threshold arises dynamically.

The Refraction Phenomenon in *Chara* Can Be Simulated Assuming An Inactivated Channel State with a Long Lifetime

Figure 5 illustrates a qualitative simulation of Ca^{2+} responses due to periodic stimulations. Employing a driver with a long period (30 sec), the response of the system is very regular (Fig. 5*A*). Decreasing the pulse period results in a more irregular $[Ca^{2+}]_{cyt}$ signal (Fig. 5*C*, *D*). In detail it can be observed that the $[Ca^{2+}]_{cyt}$ responses occur with different, partly very small amplitudes. No longer does each stimulus evoke a Ca^{2+} response. Instead, only every n^{th} pulse evokes a large-amplitude response. Stimuli in between either cause small or no responses (Fig. 5*C*, *D*). In the simulations shown in Fig. 5*C*, in which the cell is stimulated with a pulse period of 10 sec, only every second pulse initiates a $[Ca^{2+}]_{cyt}$ response. Increasing the pulse frequency (Fig. 5*D*) leads to even higher values of n, including even irregular $[Ca^{2+}]_{cyt}$ responses (Fig. 6).

This complex dependence of $[Ca^{2+}]_{cyt}$ responses on stimulation frequency (Fig. 5) is known as phase-locking. We will briefly describe the theoretical phenomenon and, on this basis, compare model simulations under an external periodic stimulus with experimental data. Phase-locking phenomena are of high interest in nonlinear dynamics, as it is known that nonlinear oscillators produce extremely rich patterns of synchronization to an external periodic stimulus, where the main control parameters are the external frequency and the strength (or amplitude) of the external signal (*see* e.g., Tass, 1999; Pikovsky et al., 2001), for the general formalism and Hütt et al. (2002), for a biological example. The synchronization between $[Ca^{2+}]_{cyt}$ and the external stimulus observed here in the amplitude response can be classified in

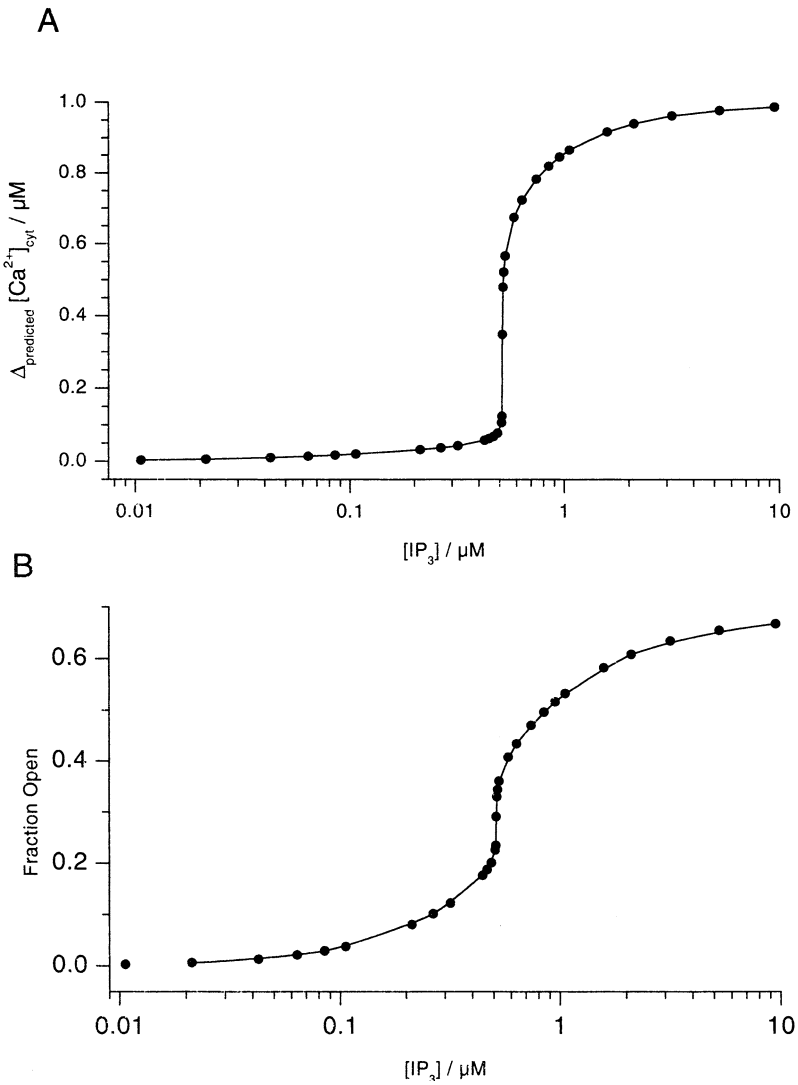

Fig. 4. The threshold is defined by a critical IP_3 concentration. (*A*) From 37 simulations and such as in Fig. 2 with pulse strength between 0 and 25 µA, the maximal $\Delta[Ca^{2+}]_{cyt}$ was obtained and plotted as a function of the maximal $[IP_3]$ calculated in the same simulations. (*B*) Plot of the fraction of open channels (x_4) as function of maximal $[IP_3]$.

terms of such phase locking. One basically counts, how many periods (say, n) of the external driving force (i.e., the current pulses) pass, before the cycle of the internal oscillator (seen in the $[Ca^{2+}]_{cyt}$) repeats. If such a relation between the external and internal oscillator exists, it is called an n:1 phase locking.

It should be noted that some of these phase-locking responses will be lost in simulations, when parameter values are changed by more than 5 percent. In spite of such limited robustness in parameter space of some phase-locking effects, we nevertheless could show that a good agreement between theory and experiment can be obtained with parameter values, which are reasonable from a physiological point of view. Further (experimental and theoretical) studies are necessary to find reliable ranges of parameters, in particular, as most of the parameter values used here are obtained from completely different systems, namely animal cells, rather than plant cells as *Chara*.

Figure 7 illustrates experimental findings on periodic stimulations, which were conducted according to model predictions. The data show that periodic stimulation of a *Chara* cell leads to Ca^{2+} responses very similar to those predicted by the model. The responses are regular if the pulse interval is sufficiently long (Fig. 7*A*). Decreasing the pulse period (Fig. 7*B*: 20, *C*: 10, *D*: 5 sec) results in an increasingly complex $[Ca^{2+}]_{cyt}$ response: The amplitude of the $[Ca^{2+}]_{cyt}$ peaks vary and different types of phase-locking can be observed, beginning with 2:1 phase-locking (*B*, *C*). In Fig. 7*D*, three or more driver periods are necessary for the $[Ca^{2+}]_{cyt}$ curve to return to the beginning of its cycle (3:1 phase-locking).

The good agreement between experimental data and model simulations allows to examine now the mechanisms underlying individual reaction steps in excitation on a more molecular basis. As an example we study here the dependence on the model parameter k_{-3}, i.e., the reaction step responsible for the inactive state of the Ca^{2+} release channel.

Figure 8*A* illustrates the role of k_{-3} on the refraction period. In the range of values shown in the

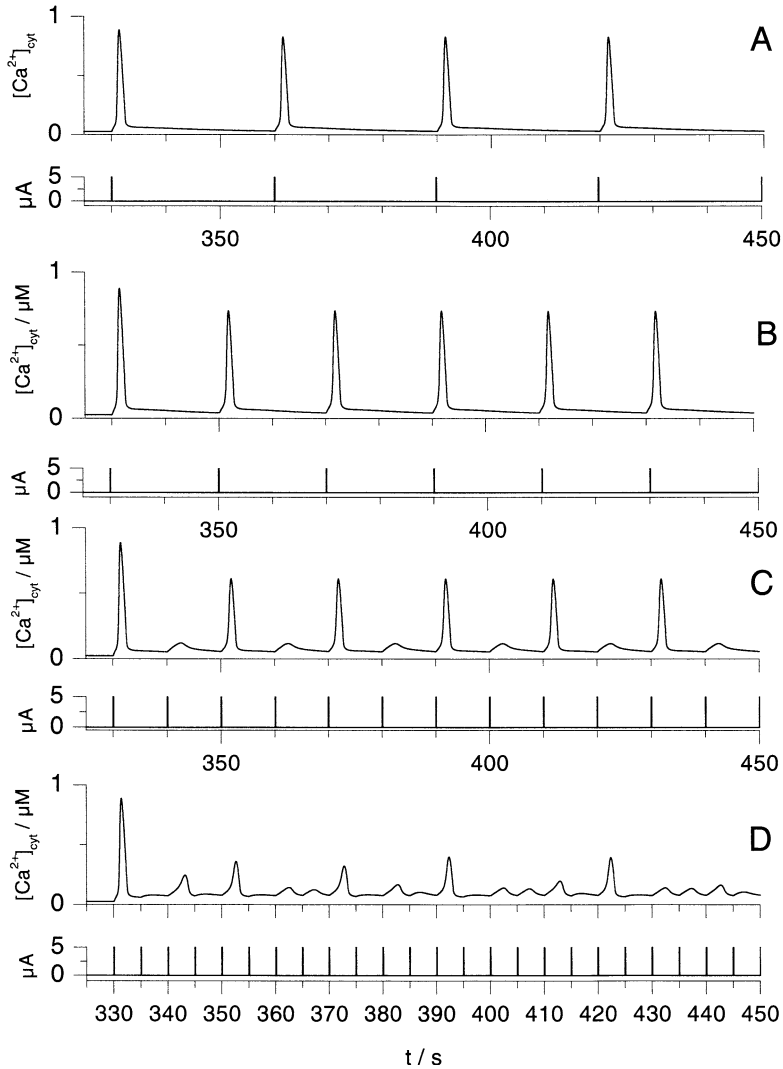

Fig. 5. Simulated Ca^{2+} responses evoked by periodic stimulation with decreasing period. Shown are parts of time courses, which were simulated with the parameters listed in Table 1 with k_{-3} = 0.086 sec^{-1}. The stimulation periods were 30 sec (*A*), 20 sec (*B*), 10 sec (*C*), and 5 sec (*D*). The pulse duration was 100 msec and the integration step size, 0.001 sec. For the first 330 sec of the simulation the system was allowed to equilibrate.

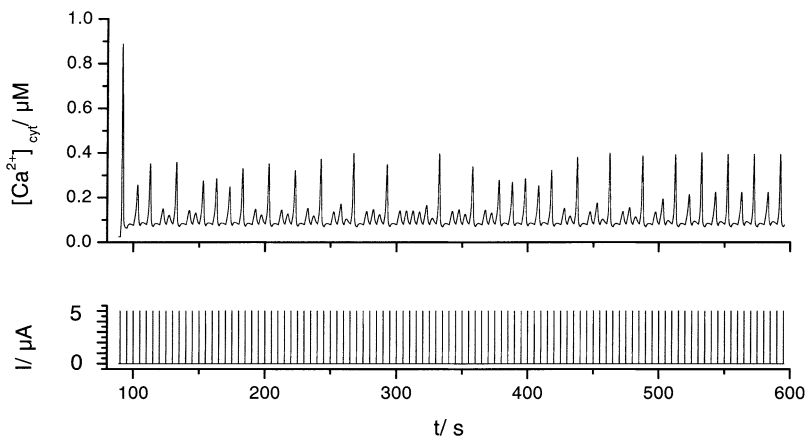

Fig. 6. Simulated Ca^{2+} responses evoked by 75 periodic stimulations. Model parameters are the same as in Fig. 5*D*.

simulation, k_{-3} has no appreciable effect on the Ca^{2+} response to the leading pulse. When k_{-3} is sufficiently high, also the trailing pulse applied 10 sec after the leading pulse is effective to stimulate a large Ca^{2+} response. However, the amplitude of the response to the trailing pulse decreases dramatically with a decrease in the value of k_{-3}. This means that the rate constant k_{-3} determines the length of the refraction

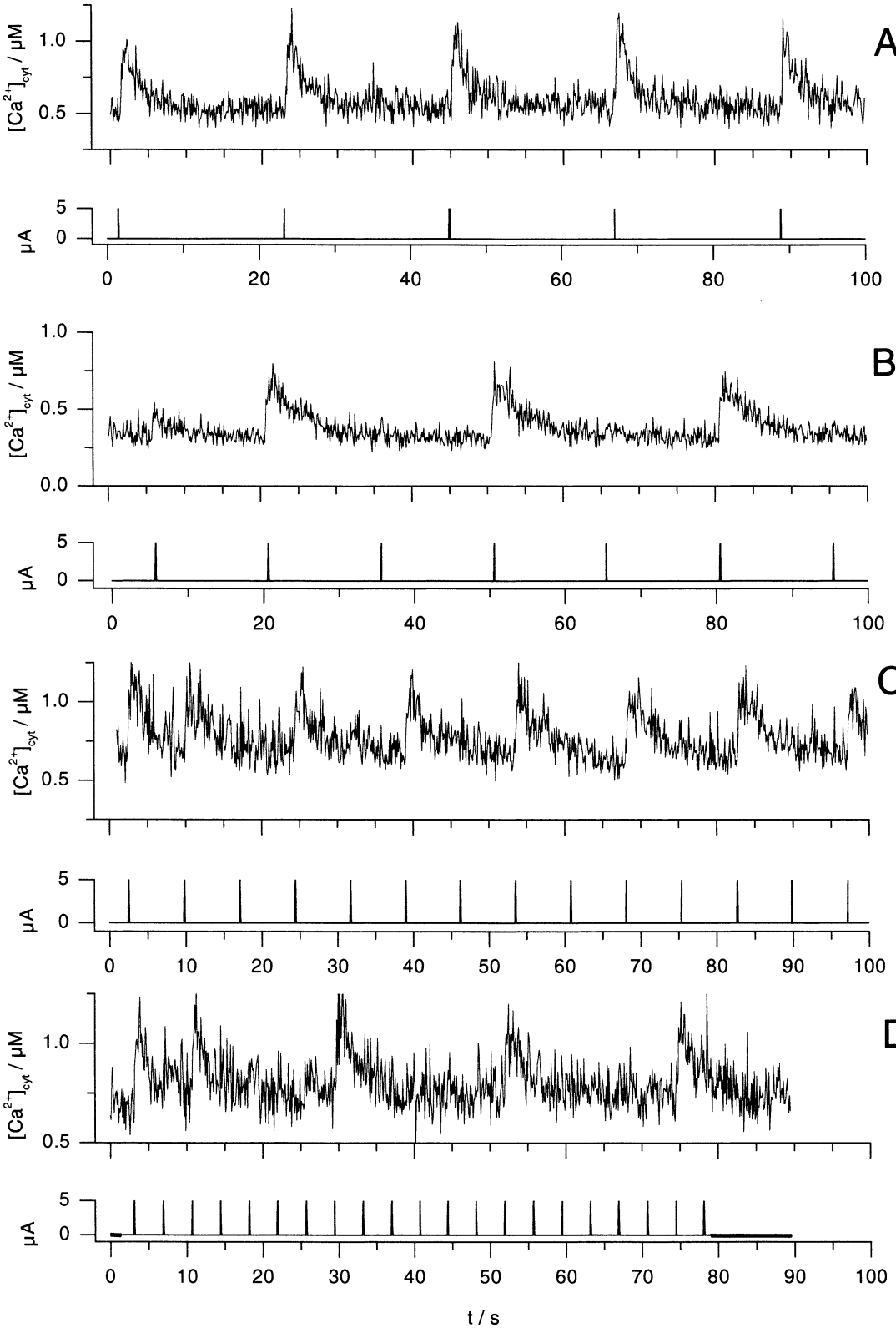

Fig. 7. Measured Ca^{2+} transients evoked by periodic stimulation with decreasing period. Shown are parts of time courses recorded with a single cell. The stimulation periods were 30 sec (*A*), 20 sec (*B*), 10 sec (*C*), and 5 sec (*D*). The pulse durations were 100 msec and the sample frequency was 10 Hz. The presentation of the data includes a small time error due to short software interrupts for data logging.

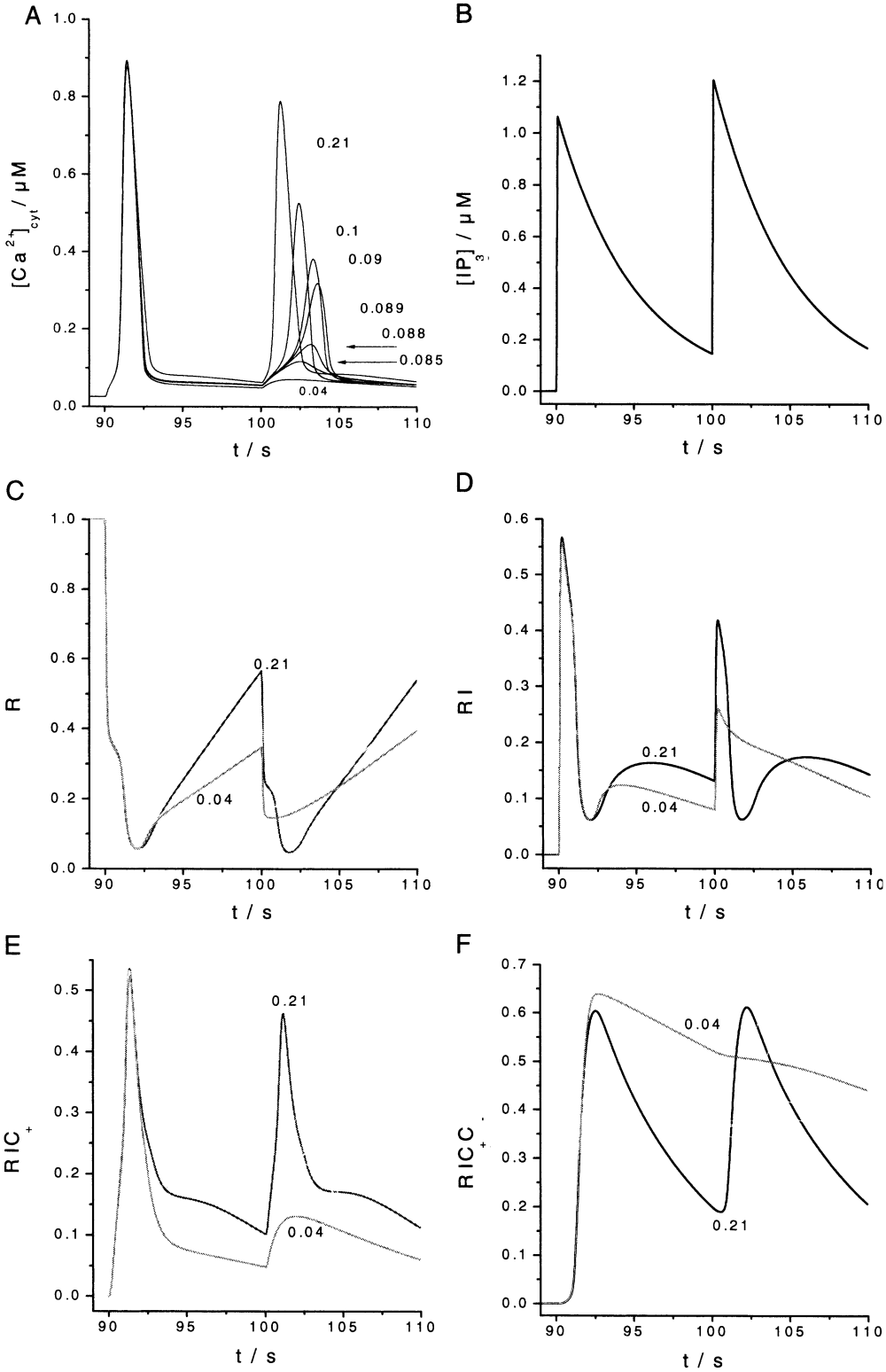

Fig. 8. Effect of k_{-3} on simulated Ca^{2+} responses. The plots show simulated Ca^{2+} transients (*A*) and the dynamics of the five system parameters (*B–F*) in response to two pulses (5 µA/100 msec) applied with 0.1 Hz. The respective values of k_{-3} are listed with the corresponding trajectories. The largest value was taken from Othmer (1997) and decreased stepwise. For remaining parameters, *see* Table 1. Periodic stimulation was started after a time of 90 sec during which the system was allowed to equilibrate. Reduction of k_{-3} has only minor effects on the leading Ca^{2+} response but dramatically decreases the trailing response, effectively making the cell refractory.

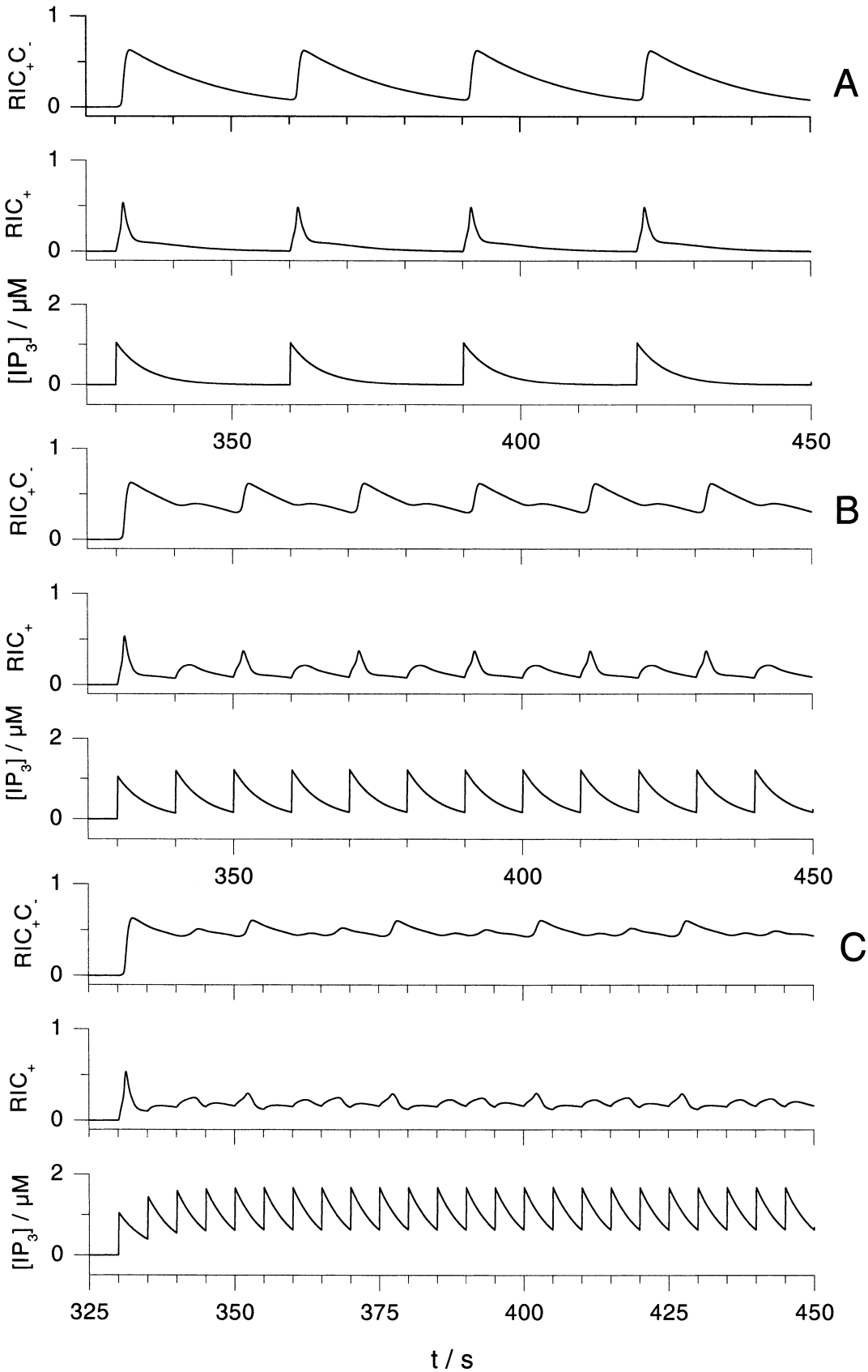

Fig. 9. Simulated dynamics of $[IP_3]$ (*bottom traces*), activated state RIC_+ (*middle traces*) and inactivated state RIC_+C_- (*top traces*) of the IP_3-gated Ca^{2+}-release channel in response to different stimulation periods. Stimulation with pulses of 5 µA amplitude and 100 msec duration occurred with periods of 30 sec (*A*), 10 sec (*B*), and 5 sec (*C*), respectively. For the other parameters, *see* legend of Figure 5.

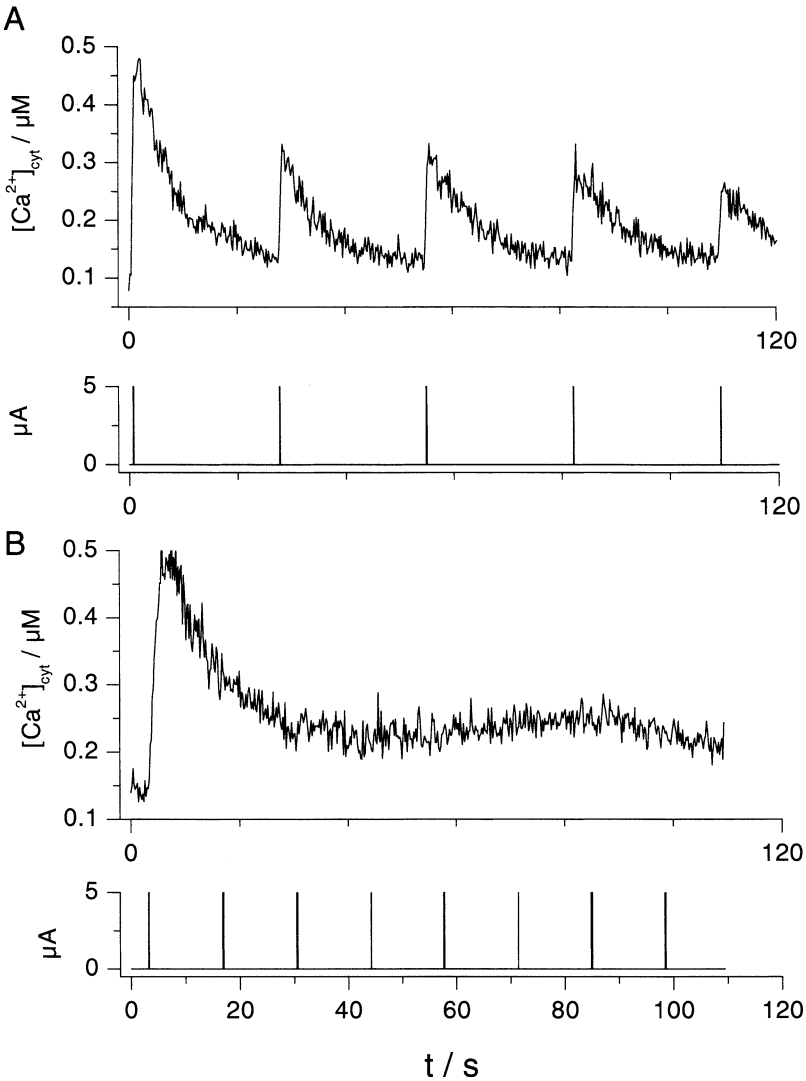

Fig. 10. *Chara* cells fail to exhibit repetitive Ca^{2+} responses if stimulated with too high a frequency. Shown are the measured Ca^{2+} responses of a *Chara* cell stimulated with a pulse period of 30 sec (*A*) and 15 sec (*B*). The presentation of the data includes a small time error due to short software interrupts for data logging. The pulse duration was 100 msec and the sample frequency, 10 Hz.

period. The effect of k_{-3} on all five system parameters can be seen in Fig. 8*B–F* in which the temporal development of the parameters is shown for the two extreme cases with $k_{-3} = 0.21$ sec^{-1} and $k_{-3} = 0.04$ sec^{-1} respectively. The predominant effect of a small k_{-3} is the lengthening of the inactive state of the channel (RIC_+C_-) which limits the number of channels in the active form RIC_+.

More details for the role of k_{-3} on the refraction period become apparent from the simulation of periodic stimulations (Fig. 9). The low value of k_{-3} (here 0.086 sec^{-1}) leads to a long-lived inactive state of the channel (RIC_+C_-). When the period of the stimulation is sufficiently long, (*A*) the respective channels can recover from the inactive state, before the onset of the next pulse. If the interval between two pulses is shorter (*B*) only every second pulse evokes an appreciable Ca^{2+}_{cyt} response, because the pulse interval is not long enough to allow full recovery from the inactive state RIC_+C_-. For even shorter pulse intervals, stimulation of the cell is for the same reason even less effective (*C*). This occurs even though the mean $[IP_3]$ rises during high-frequency stimulation much higher than during low-frequency stimulation (*A* and *B*).

Notably, a further consequence of high frequency stimulation is that ineffective pulses keep, by maintaining a high level of $[IP_3]$, the fraction of the inactivated channels high and the fraction in the activated state low (Fig. 9*C*). Under this condition, channels in the active state are more likely to shift to the long-lived inactive state (RIC_+) than to the intermediate (*RI*) state. The reason for this is that the concentration of the intermediate state *RI* is high due to the permanent high level of $[IP_3]$.

Figure 10 shows a typical experimental record of a cell, which lost excitability under a regular stimulation with a pulse period of 15 sec, while the same cell exhibited regular Ca^{2+}_{cyt} responses when stimulated

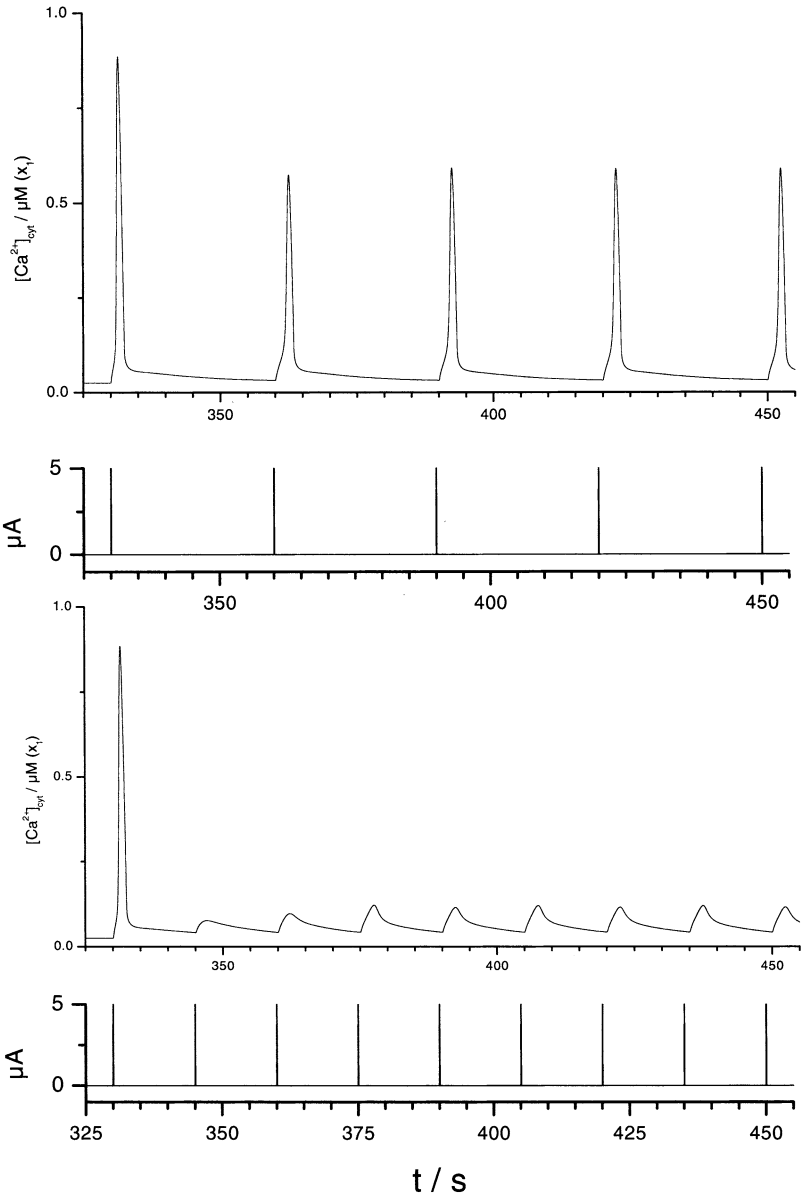

Fig. 11. Simulation of the effect of too short a stimulation period. *A* and *B* simulated with $k_{-3} = 0.04$, a pulse duration of 100 msec and an integration step size of 0.001. (*A*) With a stimulation period of 30 sec, each pulse evoked a Ca^{2+} response. (*B*) Decreasing the stimulation period to 15 sec abolished any further Ca^{2+} transients.

with a pulse period of 30 sec. In a simulation we could reproduce this effect using a value of 0.04 sec^{-1} for k_{-3}. The plot in Fig. 11*A* illustrates that driving the system with a period of 30 sec (*A*) leads to a regular, strong Ca^{2+} responce. On the other hand, stimulation with a period of 15 sec (*B*) produces a single Ca^{2+} response at the first pulse and further on only responses with small peaks. Most likely such small Ca^{2+} responses would be unresolved within the noise of an experimental record such as in Fig. 10.

Altogether, simulations and experimental results presented in the Figs. 8–10 stress that the refraction period can in our model be defined by the value of k_{-3}. On the other hand, variation of k_{-3} does not affect the all-or-none kinetics for a single pulse (Fig. 8). When a single pulse meets the system in equilibrium, all receptors are in the unbound state (*R*), and Ca^{2+} is liberated from the stores when the receptors are shifted to the active state (RIC_+). Ca^{2+} liberation is then terminated as the consequence of the receptor going into the inactive state (RIC_+C_-). When within the refraction period the system is challenged by a second pulse, most of the channels are still inactive, because of the longlife time of the (RIC_+C_-).

In addition to confirming the experimental findings, the model simulations also predict more complex types of phase-locking at even higher frequencies and, finally, a sequence of peaks with chaotic amplitude (Fig. 6). Note that, even though a 2:1 phase-locking can be found, we did not obtain any of these more complex dynamics in the original model by Othmer (1997). The simulation provides excellent guidelines for further experimental studies focusing on finding these forms of dynamics, which, as to be

expected in higher forms of phase-locking, only exist in rather small regions in parameter space.

Conclusions

Experimental research on electrical excitation in plants has over years collected a vast number of empirical observations, which remained largely unexplained in terms of the underlying mechanisms. These observations include a refractory behavior with variable times (Beilby & Coster, 1979), complete loss of excitability after frequent stimulation (Homann & Thiel, 1994) and a threshold for voltage-stimulated Ca^{2+} mobilization (Wacke & Thiel, 2001).

A large body of experimental evidence has precluded that voltage-dependent Ca^{2+} influx via plasma membrane channels can be the primary source for the rise in Ca^{2+} during excitation in *Chara* (Homann & Thiel, 1994; Thiel et al., 1997; Plieth et al. 1998; Wacke & Thiel, 2001). The experimental data on the dynamics of $[Ca^{2+}]_{cyt}$ as well as on the gating of the Ca^{2+}-sensitive Cl^- channels, which produce the depolarization of the action potential, can be best explained by a model in which a voltage-dependent production of a second messenger (Homann & Thiel, 1994; Thiel & Dityatev, 1998; Wacke & Thiel, 2001), most likely IP_3 (Thiel et al., 1990; Biskup et al., 1999), is triggering the release of Ca^{2+} from internal stores. The above analysis of a combined model for voltage-dependent production of such a second messenger and Ca^{2+} mobilization from internal stores by IP_3 and Ca^{2+} now allows successful simulation of the aforementioned body of experimental observations in the context of electrical excitation in plants. First, the model simulations show in essence that the experimentally determined threshold for the mobilization of Ca^{2+} from internal stores results from the interplay between some of the dynamical model variables. Hence it is an intrinsic threshold in the model.

In other plant systems, a cooperative binding of an activator to a channel protein was proposed in order to explain the steep dependency of a channel on an activator (e.g., Bauer et al., 1998). Such a cooperative binding with a higher-order Hill coefficient is also required in the present model (Eq. 2) to account for the steep dependency of the Ca^{2+} response on stimulation. However, while a cooperative binding site for a Ca^{2+} channel activator may be sufficient for explaining the dependency of $\Delta[Ca^{2+}]_{cyt}$ on the strength/duration of stimulating pulses, it is not sufficient to account for the complex dynamic features of membrane excitation and refractory behavior in *Chara*.

The analysis of the present model, which includes the interplay of Ca^{2+} and IP_3, provides a plausible explanation for the refractory period. Central in this process could be the lifetime of the inactivated state RIC_+C_- of the Ca^{2+} release channel, in which the channel has bound Ca^{2+} and IP_3. An appreciable Ca^{2+} release is only possible once the channel has recovered from this long-lived inactive state. So, at intermediate stimulation frequencies, the refractory time depends on the relaxation of the channel from this inactive state back into the ground state. At high frequency stimulation, the recovery of the channel is further antagonized by an elevated background concentration of IP_3 in the cytoplasm, which derives from IP_3 production due to frequent stimulation. This scenario provides a plausible explanation for the loss of excitability in response to high-frequency stimulation.

The present model is to a large extent based on the assumption that plants posses IP_3-gated channels on endomembranes and that these channels have a similar gating dependence on IP_3 and Ca^{2+} as their animal analogs. The first assumption is well founded on molecular and functional evidences. These reveal that plants possess the key proteins and mechanisms for a stimulus-induced and IP_3-mediated mobilization of Ca^{2+} from internal stores (Sanders, Brownlee & Harper, 1999; Reddy, 2001). Also *Chara* cells most likely have such a signalling system, because it was shown that electrophoretic injection of IP_3 triggered membrane excitation (Thiel, MacRobbie & Hanke, 1990), while inhibition of phospholipase C abolished excitability of these cells (Biskup et al., 1999).

On the other hand, little was so far known about the gating properties of the postulated IP_3-activated Ca^{2+} channels in plants. Efflux assays with isolated microsomes or patch-clamp measurements on isolated vacuoles have uncovered activation of Ca^{2+} release with an affinity to IP_3 comparable to that in animal cells (Muir & Sanders, 1997). On the other hand, a Ca^{2+} dependence of this process as in animal cells was so far not detected (Allen & Sanders, 1994) although such a dependence had been anticipated from the observations of Ca^{2+} oscillations in plant cells (Sanders et al., 1999).

One of the two main components of our model has been transferred from the animal to the plant case without any modification either of structure or parameter values. Most astonishingly, this construct is capable of reproducing the wide variety of experimental observations as described above. This strongly suggests that the underlying mechanisms in *Chara* are similar to the animal case discussed by Tang et al. (1996) and Othmer (1997). In particular, a central feature in this model simulation is the particular IP_3- and Ca^{2+}-sensitive gating of the respective Ca^{2+} channels. This fosters the hypothesis that the respective Ca^{2+} channels in *Chara* have the same gating properties as their animal analogue.

We are indebted to H. Busch for providing us with a first implementation of the Othmer model. Support by Deutsche Forschungsgemeinschaft to MTH and GT is gratefully acknowledged.

References

Allen, G.J., Sanders, D. 1994. Osmotic stress enhances the competence of *Beat vulgaris* vacuoles to respond to inositol 1,4,5-trisphosphate. *Plant Journal* **6:**687–695

Bauer, C.S., Plieth, C., Hansen, U.-P., Simonis, W., Schönknecht, G. 1998. A steep Ca^{2+}-dependency of a K^+ channel in a unicellular green alga. *J. Exp. Bot.* **49:**1761–1765

Beilby, M.J., Coster, H. 1979. The action potential in *Chara corallina* III. The Hodgkin-Huxley parameters for the plasmalemma. *Aust. J. Plant. Physiol.* **6:**337–353

Biskup, B., Gradmann, D., Thiel, G. 1999. Calcium release from IP_3-sensitve stores initiates action potential in *Chara*. *FEBS Letters* **453:**72–76

Homann, U., Thiel, G. 1994. Cl^- and K^+ channel currents during the action potential in *Chara;* simultaneous recording of membrane voltage and patch currents. *J. Membrane Biol.* **141:**297–309

Hütt, M.-Th., Rascher, U., Beck, F., Lüttge U. 2002. Period-2 cycles and 2:1 phase locking in a biological clock driven by temperature pulses. *J. Theor. Biol.* **217:** 383–390

Muir, S.R., Sanders D. 1997. Inositol 1,4,5-Trisphosphate-sensitive Ca^{2+} release across nonvacuolar membranes in Cauliflower. *Plant Physiology* **114:**1511–1521

Othmer, H.G. 1997. Signal transduction and second messenger Systems. *In*: Case studies in Mathematical Modeling — Ecology, Physiology and Cell Biology. H.G. Othmer, F.R. Adler, M.A. Lewis, J. Dallon, editors. Prentice Hall, Englewood Cliffs, NJ.

Pikovsky, A. 2001. Rosenblum M., Kurths J. Synchronization — A Universal Concept in Nonlinear Sciences. Cambridge University Press.

Plieth, C., Sattelmacher, B., Hansen, U.-P., Thiel, G. 1998. The action potential in *Chara*: Ca^{2+} release from internal stores viszualized by Mn^{2+} induced quenching of fura dextran. *Plant J.* **13:**167–175

Press, W., Flannery, B.P., Teukolsky, S.A., Vettilig, W.T. 1992. Numerical Recipes in C: The Art of Scientific Computing. 2nd edition. Cambridge University Press, Cambridge, New York.

Reddy, A.S.N. 2001. Calcium: silver bullet in signaling. *Plant Science* **160:**381–404

Sanders, D., Brownlee, C., Harper, J.F. 1999. Communicating with calcium. *The Plant Cell* **11:**691–706

Tang, Y., Stephenson, J., Othmer, H.G. 1996. Simplification and analysis of models of calcium dynamics based on $InsP_3$-sensitive calcium channel dynamics. *Biophys. J.* **70:**246–263

Tass, P.A. 1999. Phase resetting in medicine and biology: stochastic modelling and data analysis, Springer Verlag, Heidelberg

Tazawa, M., Shimmen, T., Mimura, T. 1987. Membrane control in the Characeae. *Annu. Rev. Plant Physiol.* **38:**95–117

Thiel, G., MacRobbie, E.A.C., Hanke, D.E. 1990. Raising the intracellular level of inositol 1,4,5-trisphosphate changes plasma membrane ion transport in characean algae. *EMBO J.* **9:**1737–1741

Thiel, G., Dityatev, A. 1998. Transient activity of excitatory Cl^- channels in *Chara:* evidence for quantal release of a gating factor. *J. Membrane Biol.* **163:**183–191

Thiel, G., Homann, U., Plieth, C. 1997. Ion channel activity during the action potential in *Chara:* A new insight with new techniques. *J. Exp. Bot.* **48:**609–622

Wacke, M., Thiel, G. 2001. Electrically triggered all-or-none Ca^{2+} liberation during action potential in the giant alga *Chara*. *J. Gen. Physiol.* **118:**11–21